ACS APPLIED MATERIALS & INTERFACES

Research Article

www.acsami.org

Artificial Peroxidase/Oxidase Multiple Enzyme System Based on Supramolecular Hydrogel and Its Application as a Biocatalyst for Cascade Reactions

Rui Qu, Liangliang Shen, Aoting Qu, Ruolin Wang, Yingli An, and Linqi Shi*

State Key Laboratory of Medicinal Chemical Biology, Key Laboratory of Functional Polymer Materials, Ministry of Education, Institute of Polymer Chemistry, Collaborative Innovation Center of Chemical Science and Engineering (Tianjin), Nankai University, Tianjin, 300071, China

Supporting Information

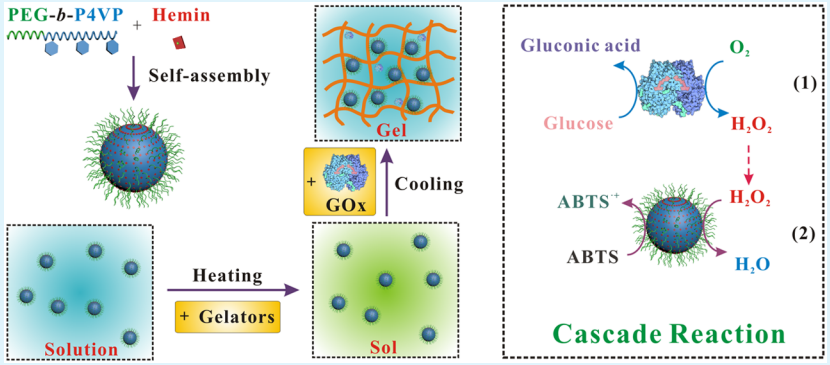

ABSTRACT: Inspired by delicate structures and multiple functions of natural multiple enzyme architectures such as peroxisomes, we constructed an artificial multiple enzyme system by coencapsulation of glucose oxidases (GOx) and artificial peroxidases in a supramolecular hydrogel. The artificial peroxidase was a functional complex micelle, which was prepared by the self-assembly of diblock copolymer and hemin. Compared with catalase or horseradish peroxidase (HRP), the functional micelle exhibited comparable activity and better stability, which provided more advantages in constructing a multienzyme with a proper oxidase. The hydrogel containing the two catalytic centers was further used as a catalyst for green oxidation of glucose, which was a typical cascade reaction. Glucose was oxidized by oxygen (O_2) via the GOx-mediated reaction, producing toxic intermediate hydrogen peroxide (H_2O_2). The produced H_2O_2 further oxidized peroxidase substrates catalyzed by hemin-micelles. By regulating the diffusion modes of the enzymes and substrates, the artificial multienzyme based on hydrogel could successfully activate the cascade reaction, which the soluble enzyme mixture could not achieve. The hydrogel, just like a protective covering, protected oxidases and micelles from inactivation via toxic intermediates and environmental changes. The artificial multienzyme could efficiently achieve the oxidation task along with effectively eliminating the toxic intermediates. In this way, this system possesses great potentials for glucose detection and green oxidation of a series of substrates related to biological processes.

KEYWORDS: *multiple enzyme system, artificial peroxidase, oxidase, cascade reaction, self-assembly*

1. INTRODUCTION

Enzymes are macromolecular biocatalysts, which are involved in many biological processes in living organisms. Most enzymes work together in multiple step reactions, in which the product of one enzyme is the substrate of the other. Cooperating enzymes often localize in the same compartment and associate in macromolecular complexes.[1] Peroxisomes are nanosized organelles that contain a variety of antioxidant enzymes with important metabolic and catabolic functions.[2−4] Oxidase is a series of highly specific enzymes, which can catalyze oxidation of specific substrates such as glucose (glucose oxidase), uric acid (urate oxidase), and reactive oxygen species (superoxide dismutase) by molecular oxygen, producing toxic intermediates such as H_2O_2. Catalases can decompose H_2O_2 specifically and prevent its damage to cellular components. Close and structured confinement minimizes the diffusion of intermediates among the enzymes, thus enhancing the overall reaction efficiency and specificity.[5]

The delicate structures and diverse functions of peroxisomes have attracted much attention for constructing multiple enzyme systems. The cascade process can be activated when enzymes are immobilized on proper scaffolds since soluble enzymes are dramatically inactivated under the reaction conditions.[6,7] The immobilization of enzymes can lead to improvements in

Received: May 20, 2015
Accepted: July 15, 2015
Published: July 15, 2015

DOI: 10.1021/acsami.5b04398
ACS Appl. Mater. Interfaces 2015, 7, 16694−16705

enzyme reusability, stability, substrate specificity, and reactivity.[8,9] However, during the immobilization, enzymes are often covalently linked to the scaffold, or located in a cross-linked aggregates, which may lead to a reduction of enzyme activity. Noncovalent methods of physical encapsulation were developed to avoid the negative influence on structure and function of enzymes. Silica particles,[10] microcapsules,[11−13] and polymersomes[14,15] were all confirmed to be excellent scaffolds for enzymes, and enzymatic activity was well-regulated by spatial organization. A multienzyme co-embedded organic−inorganic hybrid nanoflower was constructed through coordination of Cu^{2+} with the amide groups in the protein backbone.[16] The close proximity of the two enzyme components in a single nanoflower reduced the diffusion and decomposition of the intermediate H_2O_2, thereby greatly enhancing the catalytic activity. Shi and co-workers have created functional enzyme nanocomplex with well-controlled enzyme composition and spatial arrangement in a core−shell configuration. A DNA-inhibitor scaffold was used to form the enzyme complex, and the complex was further encapsulated within a polymer nanocapsule. The biomimetic enzyme nanocomplexes can be used as antidotes and preventive measures for alcohol intoxication.[17]

Most of the existing multiple enzyme systems focus on bringing natural enzymes together *in vitro* using well-designed scaffolds. However, natural enzymes have some drawbacks such as high price, low stability, and easily inhibited catalytic activity under a wide range of environmental changes.[18−20] These disadvantages may be amplified when the natural enzymes are used to construct multiple enzyme system. Our research group has long been devoted to cooperative macromolecular self-assembly toward polymeric assemblies with multiple and bioactive functions.[21,22] In our previous work, an artificial peroxidase was constructed by the self-assembly of diblock copolymer poly(ethylene glycol)-*block*-poly(4-vinylpyridine) (PEG-*b*-P4VP) and hemin, which formed a functional complex micelle.[23] The micelle provides a stable carrier for insoluble hemin in aqueous media and also a similar microenvironment for hemin as HRP. The artificial peroxidase is highly effective in catalyzing oxidation of substrates such as phenols and azo compounds, along with the decomposition of H_2O_2, which could be used as an effective H_2O_2-comsuming enzyme mimic as catalase in peroxisome. In comparison with natural enzymes, hemin-micelles exhibited comparable activity and better stability, which has great potential to construct an artificial multiple enzyme system when cooperated with a proper oxidase. A well-designed scaffold is needed to load hemin-micelles and oxidases, which can preserve or even enhance the activity of the catalytic centers.

Supramolecular hydrogels have served as scaffolds for proteins and biomolecules, which are desirable for biorelated applications, because of their high water content and biocompatible network.[24−30] However, the application of supramolecular hydrogel as a scaffold for a multiple enzyme system has seldom been investigated. The role of hydrogel is not just bringing micelles and oxidases together, but also changing the diffusion mode of the nanosized particles.[31] A class of bicomponent supramolecular hydrogels has been studied, which composed of melamine and another molecule, such as di(2-ethylhexyl) phosphoric acid (DEHPA),[32] riboflavin,[33,34] and cyanuric acid derivatives.[35] The bicomponent hydrogel has moderate mechanical strength and typical controlled release property, which is an appropriate scaffold for the catalyst.

In this work, we prepared a bicomponent supramolecular hydrogel containing hemin-micelles and GOx enzyme (HCM&E) as an artificial multiple enzyme system, as shown in Scheme 1. GOx catalyzed the oxidation of glucose by O_2,

Scheme 1. Structure and Function of the Artificial Multiple Enzyme System HCM&E[a]

[a]The image of glucose oxidase was cited from Protein Data Bank (PDB entry 1gpe).

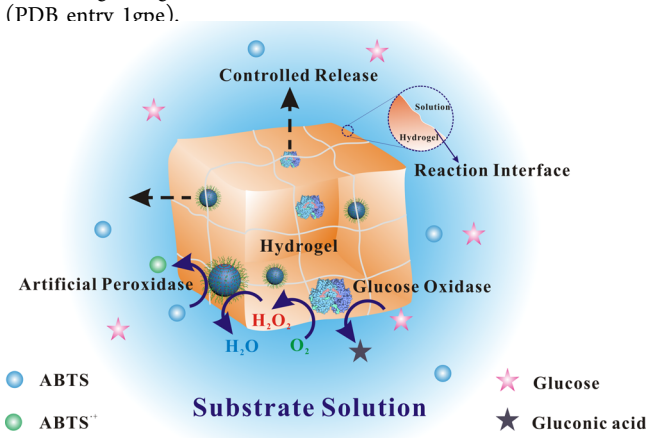

producing H_2O_2 as an intermediate product. The H_2O_2 further oxidized a chromogenic substrate, which produced a color change. The cascade reaction has mild reaction rate and high reaction efficiency. Successful integration of micelles with hydrogels combines the advantages of the two distinct biomolecule delivery platforms, which has unique benefits such as minimized burst release and controlled sequential release.[31,36−38] The hydrogel is like a protective covering for the catalyst, which protects the micelles and oxidases from inactivating by toxic H_2O_2, and also minimizes the negative effects of reaction condition on enzymatic activity. It is an innovative and groundbreaking attempt to construct a multiple enzyme system using an artificial peroxidase in cooperation with a natural oxidase, and further being co-encapsulated in a hydrogel covering. Compared with previous multiple enzyme systems, HCM&E has a simpler structure, lower preparation cost, and better protection for enzymatic activity. HCM&E can be used as a detection system for glucose and a green oxidation system for substrates such as phenols and azo compounds in aqueous media.

2. MATERIALS AND METHODS

2.1. Materials. Hemin (98%) was purchased from Energy Chemical (Shanghai, China). 2,2′-Azino-bis(3-ethylbenzothiazoline-6-sulfonate) (ABTS, 98%), Orange II (an analytical standard), di(2-ethylhexyl) phosphoric acid (DEHPA, 95%) and epigallocatechin gallate (EGCG, 98%) were purchased from Heowns Business License (Tianjin, China). Melamine (99%) and D-(+)-glucose (98%) were purchased from J&K Chemical Company (Beijing, China). Glucose oxidase (GOx) (100 units mg^{-1}) and catalase (Cat) (2000−5000 units mg^{-1}) were purchased from Sigma−Aldrich. Horseradish peroxidase (HRP) (250 units mg^{-1}) was purchased from Sanland. All the reagents were used without further purification. Poly(ethylene glycol)-*block*-poly(4-vinylpyridine) (PEG_{45}-*b*-$P4VP_{145}$) was

DOI: 10.1021/acsami.5b04398
ACS Appl. Mater. Interfaces 2015, 7, 16694−16705

synthesized in our previous work.[23] All aqueous solutions were prepared with ultrapure water (>18 MΩ) from a Millipore Milli-Q system.

2.2. Preparation of Hemin-Block Copolymer Complex Micelle. The hemin-block copolymer complex micelle was prepared according to our previous work.[23] PEG_{45}-*b*-$P4VP_{145}$ was dissolved in anhydrous *N*,*N*-dimethylformamide (DMF) with a concentration of 3 mg mL^{-1}. Hemin stock solution was prepared by dissolving hemin in 0.2 M NaOH solution with a concentration of 300 μg mL^{-1}. Then, 1 mL of polymer solution was added dropwise to 10 mL of hemin stock solution under vigorous stirring. After stirring overnight at room temperature, the mixed solution was dialyzed against 10 mM phosphate buffer (pH 7.4) (PB 7.4) for 24 h to remove DMF and to adjust the pH to neutral. The concentration of hemin-micelles refers to the concentration of hemin loaded on the micelle in this work.

2.3. Preparation of the Bicomponent Gelator. Melamine (1.27 g, 20 mmol) was dispersed in 20 mL of ethyl alcohol, and stirred for 2 h. DEHPA (3.39 g, 20 mmol) was dissolved in 10 mL of ethyl alcohol, and then added dropwise to the melamine suspension liquid within 1 h. The mixture was further stirred at room temperature overnight. The solid gelator was obtained after evaporating the ethyl alcohol at room temperature.

2.4. Preparation of Hydrogels Containing Complex Micelles (HCM) and Hydrogels Containing Complex Micelles and GOx Enzyme (HCM&E). The hydrogels were prepared by a heating−cooling process. A given volume of gelator was added into a glass tube containing different solvents. The tube was heated until the gelator completely dissolved in the solvent to achieve a sol state. The gels were formed when the sol cooled to room temperature. The compositions of the gels were shown in Table 1. Gel I was pure hydrogel without encapsulating micelles. Gel III was HCM with the same gelator concentration as Gel I. A small quantity of ethylene glycol (EG) was added to Gel I and Gel III to improve the thermal and mechanical property of the hydrogels, forming Gel II and Gel IV. The added volume of EG was much less than the main solvent, so the Gels II and IV were also considered as hydrogels in the following text.

Table 1. Recipes Used To Prepare Gels I−IV

No.	main solvent	volume (mL)	assisted solvent	volume (mL)	concentration of gelator (wt %)
I	10 mM PB 7.4	1			1
II	10 mM PB 7.4	1	EG	0.2	1
III	hemin-micelles[a]	1			1
IV	hemin-micelles	1	EG	0.2	1

[a]The hemin-micelles were prepared in 10 mM PB 7.4.

HCM&E was prepared based on HCM. GOx solution (1 mg mL^{-1}) was prepared in 10 mM PB 7.4 and stored at 4 °C. GOx solution (0.2 mL, 4 °C) was added to Gel IV in the sol state when the temperature was cooling below 70 °C, and the HCM&E was formed within a few minutes.

2.5. Release Study of Hemin-Micelle and Small Molecule Substrate. The hemin-micelle sample was prepared by mixing 1 mL of hemin-micelle (0.3 mg mL^{-1}) with 0.2 mL of EG, followed by adding 12 mg of gelator to the solution. The mixture was heated until the gelator completely dissolved in the solution, and gel was formed when it cooled to room temperature. One milliliter (1 mL) of Orange II solution (0.25 mM) was mixed with 0.2 mL of EG, and the gel was prepared using the same method as that used for the hemin-micelle sample. The gels were soaked in 2 mL of PB 7.4 (10 mM), and then hemin-micelle and Orange II began to release from the gels into the solutions. The hemin-micelle release rate was detected by measuring the absorbance at 409 nm, which was the characteristic absorption wavelength of hemin. The Orange II release rate was detected by measuring absorbance of 484 nm by using UV-vis spectra.

2.6. Catalytic Analysis. The catalytic analysis was mainly performed by a UV-vis spectrophotometer. The generated product $ABTS^{\bullet+}$ was quantitatively analyzed by measuring absorbance of 660 nm (ε = 12 mM^{-1} cm^{-1} for $ABTS^{\bullet+}$) using UV-vis spectra.[39]

The initial rate of the reaction can be obtained by the following equation:

$$\Delta c = \frac{\Delta \mathrm{Abs}}{\varepsilon b} \tag{1}$$

$$v = \frac{\Delta c}{\Delta t} \tag{2}$$

where Abs is the intensity of the absorption peak, ε the molar absorption coefficient of the product, b the optical path (the light transmittance thickness of cuvette), c the concentration of the product, t the time, v the initial rate.

The percentage conversion (Y) can be obtained by using the following equation:

$$A = c_{\mathrm{ABTS}} \varepsilon b \tag{3}$$

$$Y = \left(\frac{A_6 - A_0}{A}\right) \times 100 \tag{4}$$

where A is the theoretical absorbance of the product if the conversion rate is equal to 100%, c_{ABTS} the concentration of the substrate, ε the molar absorption coefficient of the product, and b the optical path. A_0 is the absorbance of the product at zero time and A_6 is the absorbance at the end of the reaction.

2.7. Studies of H_2O_2 Generation and Elimination. Three functional hydrogel samples were prepared, based on Gel II and Gel IV: n(GOx), n(GOx-Cat), and n(GOx-Micelle). Stock solutions of GOx, catalase, and HRP were prepared in 10 mM PB 7.4 at a concentration of 2 mg mL^{-1}. n(GOx) was prepared by adding 0.1 mL GOx stock solution and 0.1 mL PB 7.4 to Gel II in a sol state. n(GOx-Cat) was prepared by adding 0.1 mL GOx stock solution and 0.1 mL Cat stock solution to Gel II in a sol state. n(GOx-Micelle) was prepared by adding 0.1 mL GOx stock solution and 0.1 mL EGCG solution (10 mM, in 10 mM PB 7.4) to Gel IV in a sol state. The hydrogels were formed when the sol cooled to room temperature. The H_2O_2 detecting solution was prepared as follows: glucose was dissolved in 10 mM PB 7.4 at a concentration of 2 mg mL^{-1}; then, ABTS solution (5 mM) and HRP solution were added to obtain final concentrations of ABTS at 0.5 mM, glucose at 1 mg mL^{-1} and HRP at 0.1 mg mL^{-1}. The hydrogel samples were soaked in 2 mL of detecting solution. The absorbance at 660 nm (ε = 12 mM^{-1} cm^{-1} for $ABTS^{\bullet+}$) of the detecting solution was detected by a UV-vis spectrophotometer and further

DOI: 10.1021/acsami.5b04398
ACS Appl. Mater. Interfaces 2015, 7, 16694−16705

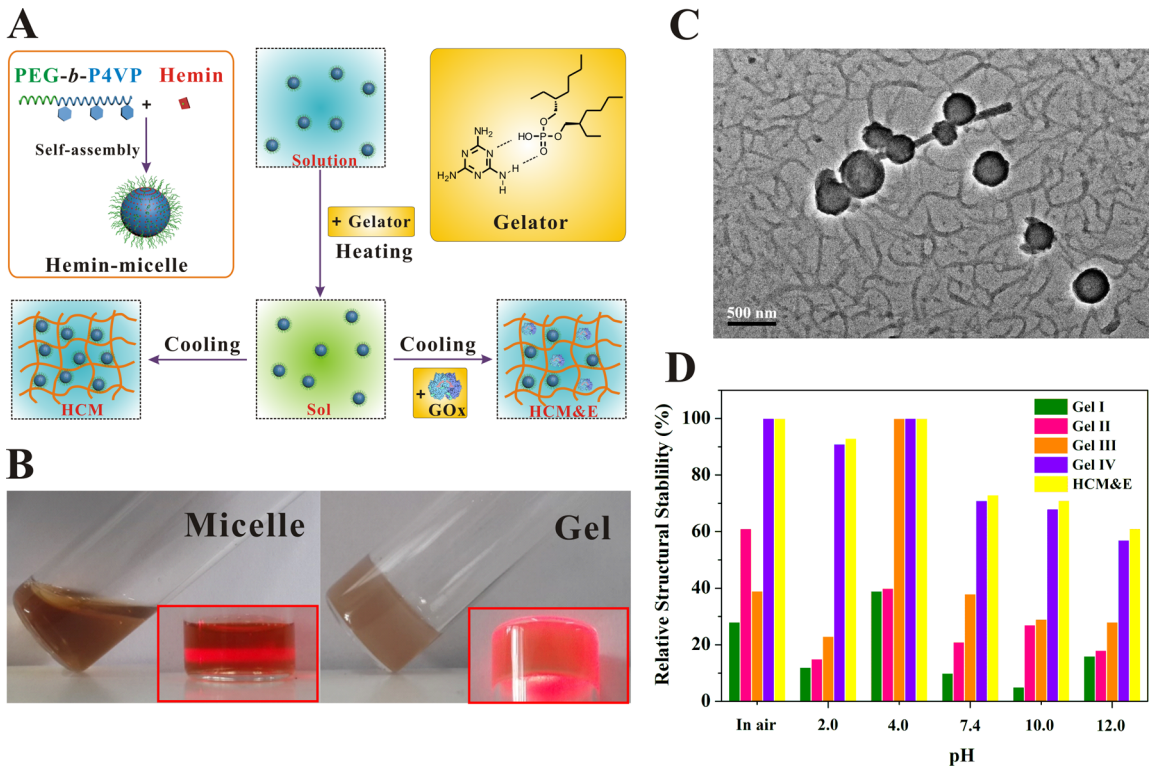

Figure 1. (A) Formations of HCM and HCM&E. (B) Photographs of the hydrogels before and after gelation; insets show laser light obtained using a simple laser generator (650 nm, 5 mW). (C) TEM image of HCM (scale bar = 500 nm). (D) Structural stability of the hydrogels in air and in solutions with different pHs. The samples were incubated at 25 °C, and the observations lasted for 10 days. The relative stability is equal to the stabilization time divided by the observation time (10 days).

transferred to H_2O_2 concentration which involved the detecting experiment.

2.8. Characterizations. Transmission electron microscopy (TEM) measurements were performed with a Tecnai G2 F20 electron microscope at an acceleration voltage of 200 kV. Samples were prepared by applying a drop of sol onto a carbon-coated copper grid, and the formed gels were dried at room temperature. Scanning electron microscopy (SEM) measurements were performed with a Shimadzu Model SS-550 electron microscope. Before imaging, the samples were sputter-coated with gold to make the samples conductive. Fourier transform infrared (FT-IR) spectroscopy was measured by Bio-Rad FTS6000 spectrophotometer at room temperature. The xerogels were obtained by freeze-drying the hydrogels. The samples were prepared by well-dispersing the complex in KBr powder and compressing the mixtures to form a plate. Dynamic laser scattering (DLS) was performed with a laser light scattering spectrometer (Model BI-200SM) equipped with a digital correlator (Model BI-9000AT) at 532 nm. All samples were prepared by filtering 1 mL of solution through a 0.45 μm Millipore filter into a clean scintillation vial and then characterizing them at 25 °C. Rheology was performed on an AR 2000ex (TA Instruments) system using a parallel plates (40 mm) at the gap of 500 μm. Rheological properties were assessed with the temperature being controlled at 25 °C using a 20 mm parallel plate geometry with a gap of 0.5 mm. The dynamic moduli of the hydrogels were measured as a function of frequency in the range of 0.1−100 rad s^{-1} with a constant strain value of 0.5%, and a function of strain in the range of 0.1%−10% with a constant frequency value of 1 Hz. UV-vis absorption spectra were measured on a Shimadzu Model UV-2550 UV-vis spectrophotometer.

3. RESULTS AND DISCUSSION

3.1. Construction and Characterization of HCM and HCM&E. Enzymes exhibit high activity and selectivity only under normal physiological conditions. Under extreme conditions, enzymes are easily inactivated either by conformation changes or other transformations of stereo chemical structure.[40] During the catalytic reaction, the solution condition changes frequently, which may lead to a reduction in the enzymatic activity. When more than one enzyme is involved in the catalytic reaction, the efficient cooperation of different enzymes becomes as important as the enzymatic activity. These problems have been considered during the construction of the artificial multiple enzyme system. An artificial peroxidase was used instead of HRP, which was an effective measure to keep the enzymatic activity at a high level.[23] The complex micelles and oxidases were encapsulated in the hydrogels; in this way, the diffusion of the catalysts was limited. The controlled release property of the hydrogel might be beneficial to the catalytic efficiency. In addition, the encapsulation of the catalysts in hydrogels is helpful to protect the enzymatic activity from some toxic products such as H_2O_2 and the extreme condition of the reaction solution.

Many attempts have been made to prepare tough hydrogels with inner cross-linking.[41,42] However, the cross-linking process is always time-consuming and has a negative effect on the enzymatic activity. The supramolecular hydrogel, which was composed of melamine and DEHPA, was prepared via a simple heating−cooling process. During the preparation process, the

DOI: 10.1021/acsami.5b04398
ACS Appl. Mater. Interfaces 2015, 7, 16694−16705

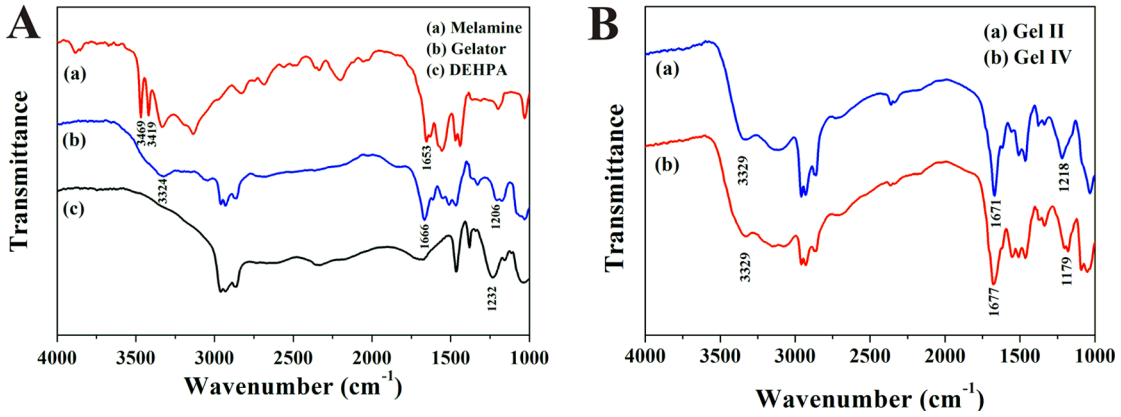

Figure 2. FT-IR absorption spectra: (A) melamine, DEHPA, and gelator; and (B) Gel II and Gel IV.

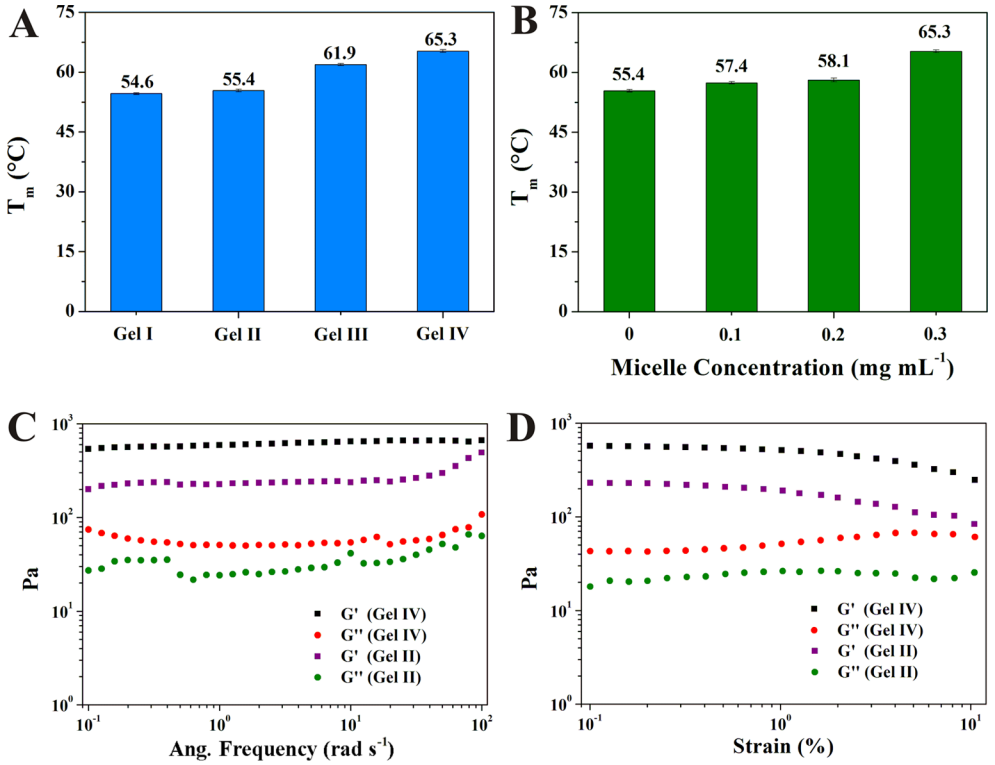

Figure 3. Melting temperature (T_m) of (A) Gel I, II, III, and IV, (B) Gel IV with different micelle concentrations. (C, D) Rheological measurements in different modes: (C) dynamic frequency sweep at a strain of 0.5% and (D) dynamic strain sweep mode at the frequency of 1 rad s^{-1}.

catalysts would suffer from high temperature (lower than 70 °C) in a few minutes, which had limited effects on the catalytic activity. Figure 1A shows the formation of HCM and HCM&E. The mass fraction of GOx in the hydrogel was <0.02%; the small quantity of oxidase may have little effect on the thermal and mechanical properties of the hydrogel. In addition, the structure of GOx is complicated, and the components of enzymes are difficult to characterize accurately. Therefore, HCM was used as a simplified model to analyze the thermal and mechanical property of the artificial multiple enzyme system.

Figure 1B shows the aggregation state of HCM during the gelation process. The hemin-micelle had good fluidity and clear Tyndall phenomenon. During the heating−cooling process, the gelators self-assembled into long fibrous aggregates, which became entangled during the aggregation process. A matrix structure was formed and further prevented the flow of solvent mainly by surface tension. The fibrous structure of the hydrogels could be observed clearly in TEM images (see Figure S1 in the Supporting Information). In Figure 1C, a hybrid structure full of fibers and spheres was observed. Both micelles and fibers preserved their own shape and structure in HCM. SEM analysis of the hydrogels was also performed, as shown in Figures S2 and S3 in the Supporting Information. There was a dramatic change in the microstructure of the hydrogels when a small quantity of ethylene glycol (EG) was added to the sol before the cooling process. The fibrous structure of Gel IV (Figure S3) was denser and much more ordered than that of Gel III (Figure S2).

The hydrogel was design to function as a catalyst in the substrate solution, which would have frequent matter exchange between the hydrogel and the solution. The structure of the hydrogel should be kept for maximum protection during the catalysis. However, the supramolecular hydrogels would swell

DOI: 10.1021/acsami.5b04398
ACS Appl. Mater. Interfaces 2015, 7, 16694−16705

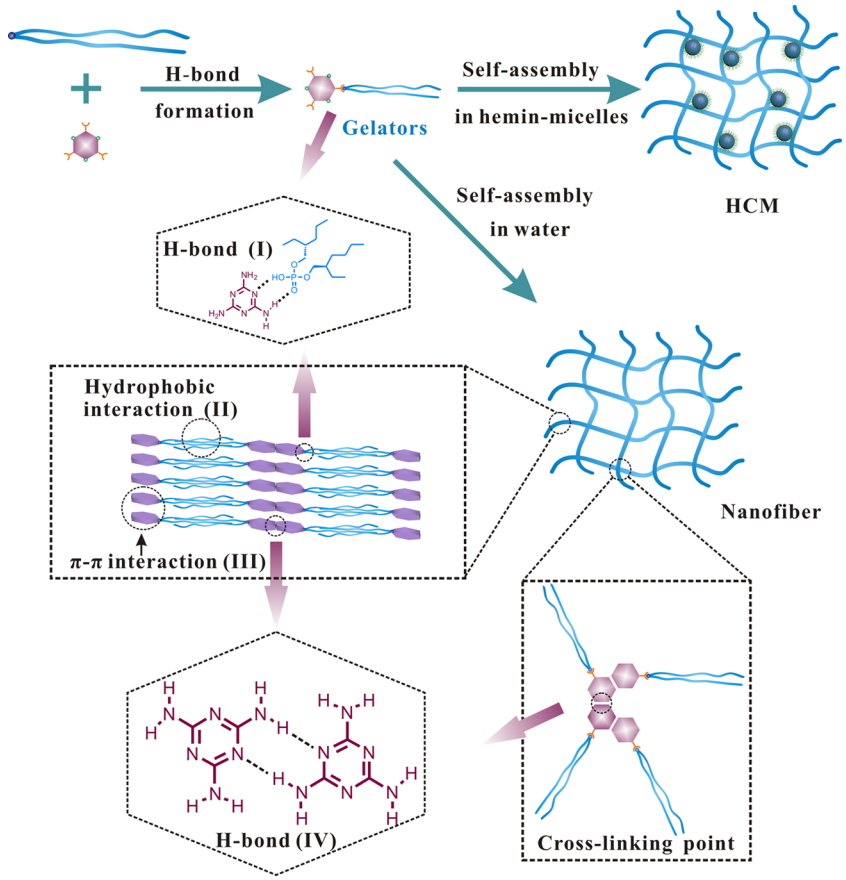

Figure 4. Possible molecular arrangements in self-assembled nanofibers of hydrogels.

or even disintegrate in solutions after a period of time. The structural stability of the hydrogels was tested by measuring the stabilization time of the hydrogels from formation to disintegration under room temperature, as shown in Figure 1D. The small quantity of EG could improve the structural stability of the hydrogels both in air and in solution. HCM (Gel IV) and HCM&E could preserve full structures in solutions with different pHs for more than a week, exhibiting satisfactory structural stabilities.

3.2. Thermal and Mechanical Property of HCM. FT-IR spectra of the gelator and xerogels were recorded to confirm the formation of hydrogen bonds (H-bond). Figure 2A shows the FT-IR spectra of melamine, DEHPA, and the bicomponent gelator. The phosphoryl (P═O) peak of pure DEHPA appeared at 1232 cm^{-1}; however, this peak shifted to 1206 cm^{-1} in the gelator, which was due to the strong H-bond involvement of the phosphoryl groups with the $-NH_2$ group of melamine. The $-NH_2$ stretching vibration peaks at 3469 and 3419 cm^{-1} in melamine were shifted to lower energy for gelator (3324 cm^{-1}), and the subsequent vibration of the heterocyclic group (−C═N−) shifted from 1653 cm^{-1} to 1666 cm^{-1}, which also proved the formation of an H-bond between DEHPA and melamine in the gelator. In Figure 2B, the stretching vibration peaks of P═O and −C═N− of Gel IV had obvious shifts compared with Gel II, which indicated that stronger H-bond was formed in the Gel IV. The detailed analysis of the interactions between hemin-micelles and gelators was included in Figure S4 in the Supporting Information.

The thermal property of the hydrogels was performed by measuring melting temperature (T_m) of the hydrogels.[43−45] The hydrogels were heated from 20 °C to 90 °C at a heating rate of 2 °C min^{-1}. The temperature at which the hydrogels began to melt and disintegrate was recorded and was denoted as T_m. The supramolecular interactions among the gelators began to collapse above T_m. In Figure 3A, the T_m values of Gel II and Gel IV were higher than those of Gel I and Gel III, respectively, which indicated that the addition of EG improved the thermal property of the hydrogels. In Figure 3B, the T_m value of Gel IV increased with the concentration of hemin-micelle changing from 0 to 0.3 mg mL^{-1}, which indicated that the encapsulated micelles can improve the thermal property of the hydrogel. The T_m of Gel IV (0.3 mg mL^{-1} hemin) was 65.3 °C, which indicated that the fibrous structure of the hydrogel was stable when the temperature was below 65.3 °C.

To investigate the mechanical properties of the hydrogels, rheological measurements were performed using dynamic frequency sweep mode and dynamic strain sweep mode. As shown in Figures 3C and 3D, both the storage modulus (elasticity of G') and the loss modulus (viscosity of G'') exhibited weak frequency and strain dependences. The G' values of all samples were bigger than the corresponding G'' values, suggesting that all samples behaved as viscoelastic materials. Gel IV showed higher G' value than that of Gel II, which indicated that the addition of hemin-micelle strengthened the hydrogel.

3.3. Possible Mechanism for Formation of HCM. Through the morphology and stability analysis, along with the exploration of the thermal and mechanical property, we proposed the possible process of the self-assembly during the formation of the hydrogel, as shown in Figure 4. In the gelator

DOI: 10.1021/acsami.5b04398
ACS Appl. Mater. Interfaces 2015, 7, 16694−16705

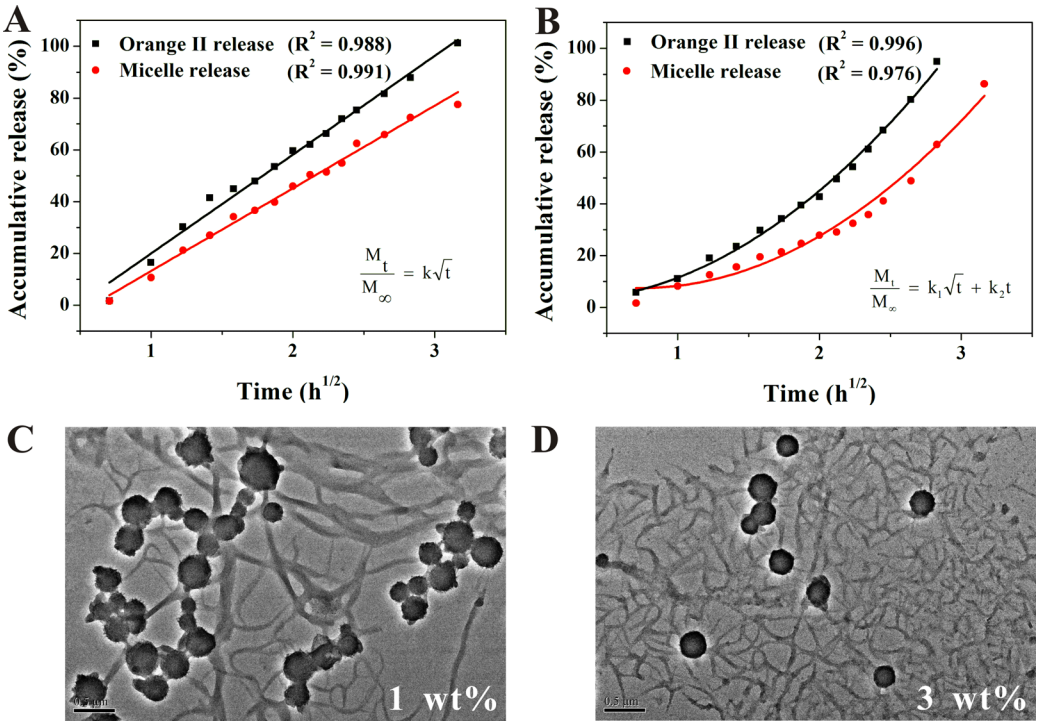

Figure 5. (A) Release percentage plotted against the square root of release time, which yielded liner fittings using Higuchi model. The concentration of the gelator was 1 wt %. (B) Nonliner fittings using a transformation of Peppas equation. The concentration of the gelator was 3 wt %. (C, D) TEM images of HCM with different concentrations of gelators: (C) 1 wt % and (D) 3 wt %. Scale bar for panels C and D: 500 nm. The release experiments were performed at 37 °C.

complex, H-bond was formed between DEHPA and melamine. The gelators can self-assemble into nanofibers in water or EG-water mixture. The formation of the liner structure was driven by H-bonding between DEHPA and melamine (I), hydrophobic interaction between DEHPAs (II), $\pi-\pi$ interaction between melamines (III), and H-bonding between melamines (IV). When more than one melamine-melamine H-bond (IV) was formed in one molecule of melamine, the fibers began to grow into a net structure because of the formation of cross-linking points among the fibers. As to HCM, the driving force to form fibrous structure was more than the interactions among the components of the gelators. The carboxyl groups of the hemin loaded on the micelles can form H-bonds with melamine and DEHPA, which made the micelles closely linked with nanofibers. The supramolecular interactions within HCM were stronger than those in hydrogels without encapsulating micelles, which could explain the reason for the better thermal and mechanical properties of HCM.

The addition of EG in the solvent can enhance the structural stability, thermal property, and mechanical stability of the hydrogel. The Flory–Huggins interaction parameter (χ) was used to evaluate the gel behavior about a known gelator in an untested solvent.[32] According to the solubility theory, the tendency toward dissolution increases as χ decreases. Solvents with low χ values may enhance the solubility of the solute, which indicates that the addition of organic solvents could prevent the precipitation of the hydrogel and thus improve the duration of the hydrogel. The detailed analysis of the solvent effect on the gelation was included in the Supporting Information.

3.4. Release Kinetics. Hydrogels are extensively studied as matrices for the controlled release of macromolecules.[46−50] The controlled release property may have great influence on the diffusion mode of the catalysts and further affect their catalytic efficiency. HCM&E functions as a multiple enzyme system when soaked in a substrate solution. The micelles and oxidases release from the hydrogel to the solution, and the substrates diffuse in the opposite direction. The diffusion modes of the catalysts and the substrates in this system are different from those in solution environment. The release kinetics of the catalysts and the substrates should be studied in order to explore the effect of the controlled release property on the catalytic efficiency of the multiple enzyme system. The hemin-micelle was used as the template for the release study about the nanosized catalysts, because the hemin loaded on the micelle is easily detected by an UV-vis spectrophotometer. Orange II was chosen as the template molecule for the substrates, which has a characteristic absorption at 484 nm.

As to the hydrogel sample with 1 wt % gelator, almost 100% of the substrates were released within 10 h, and ~80% of the hemin-micelles were released during the same time (see Figure S5 in the Supporting Information). The H-bond interaction between the micelles and the fibers reduced the release rate of the micelles. The steric hindrance of the fiber matrix for the nanosized micelle could also account for the lower release rate. Figure S6 in the Supporting Information shows the hydrodynamic diameter distribution $f(D_h)$ of hemin-micelles in the releasing solution during the releasing process. The average D_h was larger than that of the micelle before being encapsulated in hydrogel, because of the heating–cooling process during the preparation of the hydrogel.

The release was analyzed using a mathematical model established in previous hydrogel-mediated drug release studies.[51−54] It was hypothesized that the release kinetics are primarily dominated by diffusional micelles or substrates efflux with negligible contributions from the network. A diffusion-

DOI: 10.1021/acsami.5b04398
ACS Appl. Mater. Interfaces 2015, 7, 16694−16705

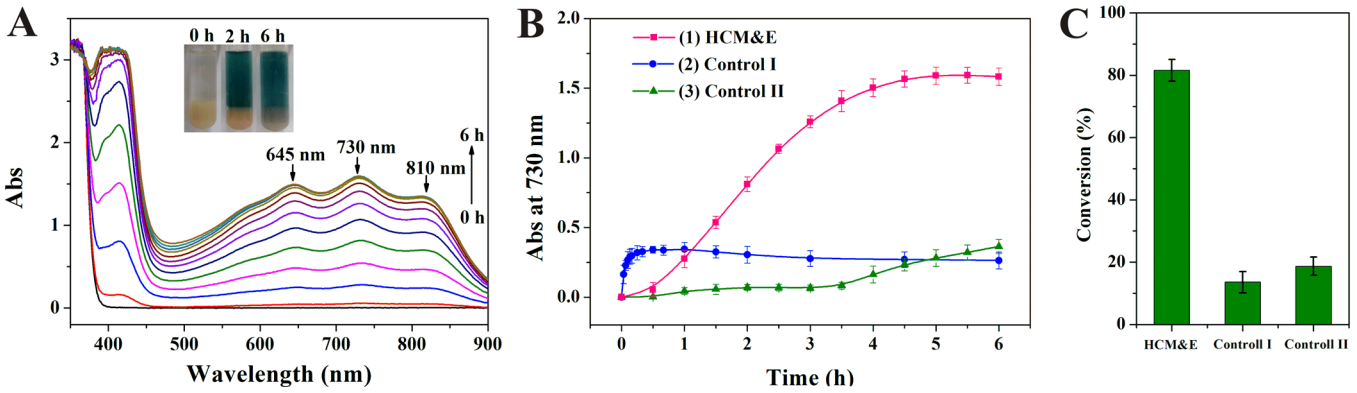

Figure 6. (A) UV-vis spectra of $ABTS^{\bullet+}$ during the oxidation reaction catalyzed by HCM&E and the color change of the solution during the reaction. The measurement was performed every half an hour, lasting for 6 h. (B) Time-dependent absorbance changes as a result of the oxidation of ABTS catalyzed by (1) HCM&E, (2) Control I, and (3) Control II. (For HCM&E, both of the hemin-micelle and GOx were encapsulated in the hydrogel. For Control I, GOx and hemin-micelles were simply mixed with substrate solution without hydrogel covering. Control II involved hemin-micelle in hydrogel and GOx in a substrate solution. All of the catalytic reactions were performed at 37 °C.) (C) Conversions of the reactions catalyzed by HCM&E, Control I, and Control II.

dominant Higuchi model was applied to analyze the release profiles:

$$M_t = Kt^{1/2} \tag{5}$$

where M_t is the rate of drug release at time t and K is the Higuchi constant. When the gelator concentration was 1 wt %, plotting the release percentage against the square root of time yielded linear fittings with a correlation coefficient of $R^2 = 0.991$ for hemin-micelle and 0.988 for Orange II, as shown in Figure 5A. The goodness of the fit indicated a diffusion-controlled release mechanism. The Higuchi constants of micelle and Orange II were calculated to be 31.9 ± 0.8 and 38.6 ± 1.1, respectively.

When the concentration of the gelator increased from 1 wt % to 3 wt %, the release rates of micelles and substrates became much lower in the first 6 h. However, the release rates increased rapidly after 6 h (see Figure S5 in the Supporting Information). The release was no longer a diffusion-dominant process, which cannot be analyzed by the Higuchi model. The releasing condition was similar to drug delivery from swellable systems, which can be expressed by the following equation:

$$\frac{M_t}{M_\infty} = k_1\sqrt{t} + k_2 t \tag{6}$$

where k_1 and k_2 are constants.[53] In Figure 5B, the goodness of the fit according to eq 6 indicated a diffusion-controlled and relaxation-controlled release mechanism.

The higher concentration of gelators led to higher fiber density of the hydrogels, as shown in Figures 5C and 5D. The hydrogel with the higher concentration of gelators had a stronger binding force for the hemin-micelles; the compact fibrous structure also slowed the diffusion rate of substrates from the solution to the hydrogel. The lower gelator concentration seemed to be more appropriate for the multiple system, since, in this state, catalysts and substrates could keep a relative high release rate in the initial stage of the cascade reaction.

3.5. Catalytic Analysis of HCM and HCM&E. The HRP-like activities of hemin-micelles and HCM were tested through the ABTS by H_2O_2, which produced dark-green ABTS cation radical ($ABTS^{\bullet+}$). The hemin-micelle solution and HCM were prepared with the same concentration of hemin (0.3 mg mL^{-1}). The two samples were mixed with the same volume of substrate solutions (0.25 mM ABTS and 12 mM H_2O_2). As shown in Figure S7 in the Supporting Information, the catalytic reaction finished within 2 min in hemin-micelle solution. When the hemin-micelles were encapsulated in the hydrogel, the reaction reached highest conversion at the 35th minute. The final reaction conversion catalyzed by HCM was higher than that by hemin-micelle solution. The porous structure of the hydrogel network permitted sufficient flexibility to assist the transports of the catalysts and the substrates, and the controlled release property of hydrogels made the catalytic reaction perform in a mild way.

With regard to HCM&E, H_2O_2 was produced during the oxidation of glucose by O_2 via a GOx-mediated reaction. The substrate solution was prepared in 10 mM PB 7.4 containing 1.0 mg mL^{-1} glucose and 0.25 mM ABTS. When the hydrogel HCM&E was soaked in the substrate solution, the cascade reaction was activated as follows:

$$\text{glucose} + O_2 \xrightarrow{\text{GOx}} \text{gluconic acid} + H_2O_2 \tag{I}$$

$$ABTS + H_2O_2 \xrightarrow{\text{Hemin-Micelles}} ABTS^{\bullet+} + H_2O \tag{II}$$

Reaction I was the oxidation of glucose, producing intermediate H_2O_2. Reaction II was the oxidation of ABTS, which was the H_2O_2-consuming reaction. Figure 6A is the absorbance change of the reaction solution over time. The absorbance at 645, 730, and 810 nm all increased, along with the reaction, indicating the production of $ABTS^{\bullet+}$. The reaction solution turned green within 1 h and the color became deeper along with the reaction, which also indicated the activation of the cascade reaction.

Figure 6B shows the time-dependent absorbance changes as a result of the oxidation of ABTS, and Figure 6C shows the conversions of the reactions. In HCM&E, the two catalytic centers were both located in the hydrogel. The cascade reaction performed under mild condition and reached a high conversion. When the micelles and enzymes were not encapsulated in hydrogels, just simply mixed with the substrate solution (Control I), the reaction finished within half an hour, and the conversion was much lower. In solution environment, no limitation on diffusion of the catalysts and substrates caused a certain degree of disorder, the two separated reactions were

DOI: 10.1021/acsami.5b04398
ACS Appl. Mater. Interfaces 2015, 7, 16694−16705

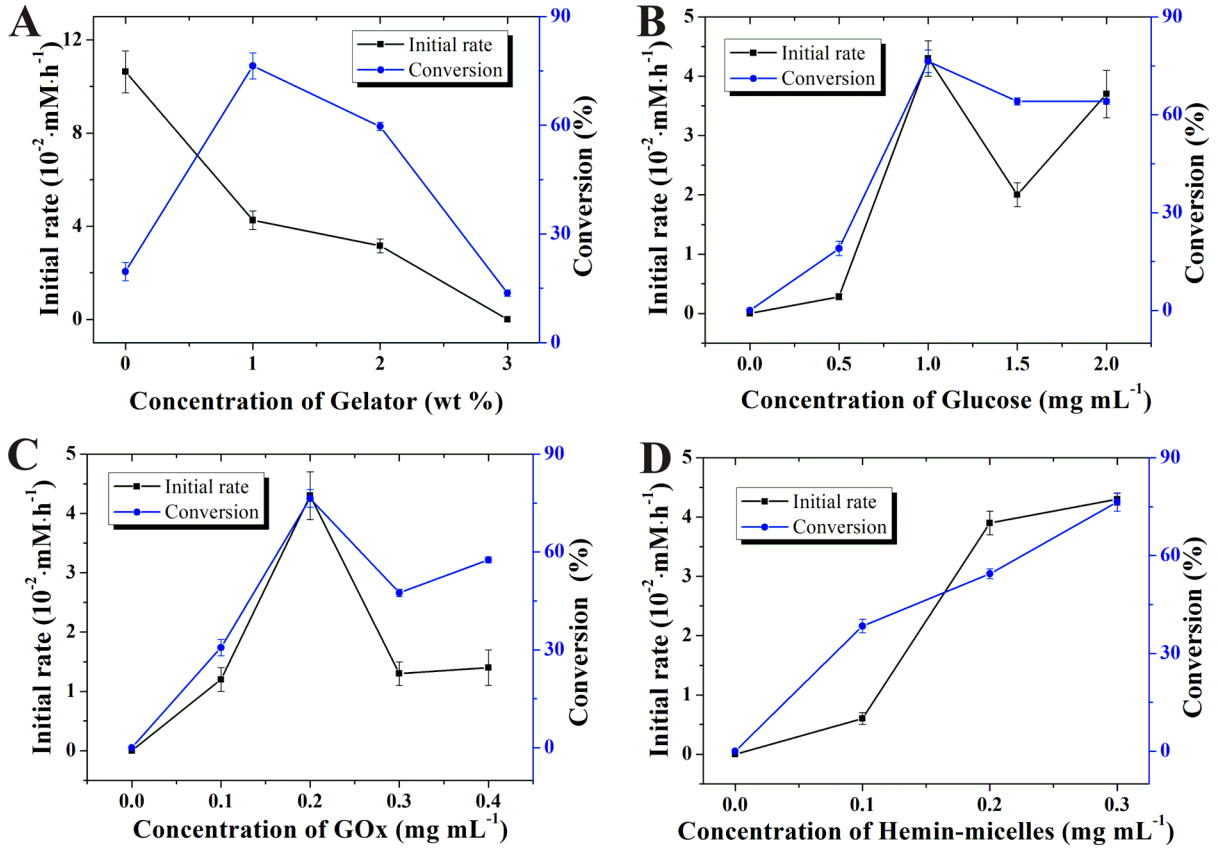

Figure 7. Initial rates and conversions of cascade reactions catalyzed by HCM&E with different concentrations of (A) gelator, (B) glucose, (C) GOx, and (D) hemin-micelle. For panels B–D, the concentration of the gelator was 1 wt %. All of the catalytic reactions were performed at 37 °C.

hard to form a cascade process. In order to further prove whether the co-encapsulation of the two catalytic centers was responsive for the high catalytic activity, the two catalysts were located in separate phases: the hemin-micelle was encapsulated in the hydrogel, and the GOx was dissolved in substrate solution (Control II). The cascade reaction was not activated until the fourth hour, and the conversion was much lower than that of HCM&E. In this system, glucose and GOx were dissolved in the same phase without limitation of their diffusion, reaction I performed at a high rate. The hemin-micelle was encapsulated in the hydrogel, the controlled release property of the hydrogel restricted the reaction rate of reaction II. The produced H_2O_2 in reaction I could not consumed by reaction II immediately, which caused a low efficiency. Some researches proved that peroxidases could be irreversibly inactivated by exposure to high concentration of H_2O_2.[55−57] The possible mechanism of the inactivation of peroxidase was analyzed in the Supporting Information (Figure S8).

3.6. Key Factors that Affected Catalytic Activities of HCM&E. The catalytic activity was measured through two parameters, namely, the initial rate (v) and the conversion rate (Y). The cascade reactions catalyzed by hydrogels with different network densities were performed, just as shown in Figure 7A. In solution environment, the mobility of the catalytic centers and substrates was highest, the cascade reactions performed at high initial rate but achieved low conversion. When the gelator concentration was 1 wt %, the cascade reaction performed smoothly and efficiently with a high conversion and a moderate initial rate. However, when the gelator concentration further increased, the initial rate and conversion both decreased. The compact network of hydrogels overly limited the diffusions of the catalytic centers and the substrates (Figure 5), thereby inhibited the cascade reaction. Based on release study and catalytic analysis above, a quantity of 1 wt % was adopted as the appropriate gelator concentration in the following analysis.

The glucose concentration varied from 0 to 2.0 mg mL^{-1}, and the catalytic activity was shown in Figure 7B. According to the catalytic dynamics of the single reaction, the higher substrate concentration may lead to higher initial rate and conversion.[19] However, with regard to cascade reaction, the situation was different. When the concentration of glucose was 1 mg mL^{-1}, the initial rate and conversion reached the highest, which were even higher than those with higher glucose concentrations. When the concentration of GOx was chosen as a variable, the similar result was achieved, just as shown in Figure 7C. When the concentration of GOx was 0.2 mg mL^{-1}, the initial rate and conversion reaches the highest, which were higher than those with higher GOx concentrations. Next, we changed the concentration of hemin-micelles, which were the catalytic centers of the reaction II. In Figure 7D, we can see that the initial rate and conversion of the cascade reaction increased as the micelle concentration increased. Based on the above analysis, we can conclude that the high reaction rate of reaction I may not necessarily lead to a high reaction rate of the cascade reaction. The product produced in reaction I should be consumed immediately by reaction II, and the excess product of reaction I may lead to low efficiency of the cascade reaction. In addition, the excess H_2O_2 may inactivate the hemin-micelles released from the hydrogel. So the concentrations of glucose and GOx should be maintained at appropriate values, in order

DOI: 10.1021/acsami.5b04398
ACS Appl. Mater. Interfaces 2015, 7, 16694−16705

to ensure that the H_2O_2 could be consumed without delay. The concentration of hemin-micelle should be maintained at a high value in order to eliminate the H_2O_2 quickly and promote the cascade reaction.

Although it is still difficult to obtain the complete reaction details about the HCM&E system, because of current limitations on characterizations, the possible process of the cascade reaction has been investigated. The color change of the reaction system was tracked for 24 h at a relatively low temperature. As shown in Figure S9 in the Supporting Information, the interface between the hydrogel and the solution first turned green, which indicated that the cascade reaction was activated at the interface. The solution away from the interface began to turn green, because of the diffusion of the product from the interface to the solution. In addition, the catalysts that diffused into the solution could also catalyze the cascade reaction, although with lower efficiency than that of the reaction that occurred at the interface. In the first 5 h, no color change was observed in the gel phase, which indicated that (i) less products were produced there and (ii) the diffusion rate of the product into the hydrogel was slow. The reverse flows of the catalysts and substrates at the interface ensured full contact of them and greatly promoted the reaction. The controlled release property made the reactions perform in a mild and ordered way, ensuring that the H_2O_2-producing reaction and H_2O_2-consuming reaction perform at the same time. In addition, the hydrogel covering protected the catalysts from toxic products and unstable reaction conditions, which had great contributions to the high efficiency of the cascade catalysis.

3.7. Studies of H_2O_2 Generation and Elimination. A major advantage of peroxisomes is the transfer of biosynthetic intermediates between catalytic sites without or with less diffusion into the bulk phase of the cell, which is referred to as "metabolic channeling".[1,58] Oxidases are widely used for various therapeutics, but oxidase-mediated reactions produce toxic H_2O_2.[59−61] With regard to our multiple enzyme system, the produced H_2O_2 could further involve in a peroxidase-mediated reaction and successfully completed a cascade process. During the cascade reaction, the generation and elimination of the H_2O_2 should be studied in order to prove whether this "metabolic channeling" was green and nontoxic in our multiple system.

Three hydrogel samples were prepared: n(GOx), n(GOx-Cat), and n(GOx-Micelle). The net rates of H_2O_2 production were quantified by adding the hydrogel samples to a glucose−ABTS−HRP solution and measuring the absorbance of produced $ABTS^{\bullet+}$.[17] The results are shown in Figure 8. In n(GOx), H_2O_2 was produced at a constant rate, relative to time. Hemin-micelles, along with a polyphenol substrate EGCG, acted as a H_2O_2-consuming enzyme such as catalase.[62−65] The net rate of H_2O_2 production for the n(GOx-Cat) and n(GOx-Micelle) were much lower than that for n(GOx). The multiple system exhibited an excellent capability for H_2O_2 elimination, which minimized the harm of toxic H_2O_2 to the surroundings.

3.8. Potential Applications of the Artificial Multiple Enzyme System HCM&E. In our previous work, hemin-micelles proved to be efficient in catalyzing the oxidation of phenols, azo compounds, and benzidines, which provided great potentials for applications in H_2O_2 detection and industrial pollutant decontamination.[23] Large amounts of H_2O_2 were required during the oxidation reactions. However, chemical

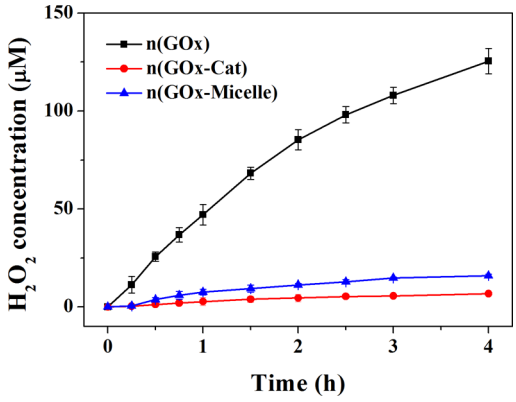

Figure 8. H_2O_2 concentration in glucose oxidation reaction catalyzed by n(GOx), n(GOx-Cat), and n(GOx-Micelle).

synthesis of H_2O_2 is not environmentally friendly, and high concentration of H_2O_2 may lead to the inactivation of peroxidases.[57,66] The HCM&E, which can produce H_2O_2 *in situ*, using glucose and molecular oxygen as green substrates, enables the quantitative oxidation of phenols, azo compounds, and some other substrates without the addition of H_2O_2. Some chromogenic substrates, such as 3,3′,5,5′-tetramethylbenzidine (TMB), catechol, and ABTS, can be oxidized by H_2O_2 via a HRP-mediated reaction, along with color changes. In this way, the HCM&E is effective in detecting glucose, when cooperated with a chromogenic substrate. The glucose can be detected not only by using the spectrophotometer but also by the naked eye, as shown in Figure 6A and Figure S9 in the Supporting Information. In this work, we performed the chromogenic cascade reaction with glucose concentration from 0.5 mg mL^{-1} to 2 mg mL^{-1}, which corresponds to the blood-glucose concentration from hypoglycemia to hyperglycemia. The glucose over the entire tested range can activate the cascade reaction (Figure 7B), which has great potential applications in bioanalysis and biological detection.

The hydrogel containing complex micelles as artificial peroxidases and GOx enzymes provides us a new view to construct multiple enzyme system mainly using the method of self-assembly instead of chemical processes. Oxidase is a series of highly specific enzymes with diverse functions, GOx is just a template enzyme, which cooperates well with hemin-micelles in the supramolecular hydrogel. The GOx can be replaced by other oxidases, such as superoxide dismutase, alcohol oxidase, and urate oxidase; thus, HCM&E may have many more applications tailored to specific physiological and environmental functions.

4. CONCLUSIONS

In summary, we report an artificial multiple enzyme system HCM&E constructed by encapsulating hemin-block copolymer complex micelle as an artificial peroxidase and GOx as a natural oxidase in a supramolecular hydrogel. The artificial peroxidase could work well with natural oxidases and exhibited excellent activity in catalyzing cascade reactions. The hydrogel serves as an excellent scaffold to carry micelles and enzymes, which protects them from inactivating by intermediate product H_2O_2. The controlled release property of hydrogel ensures the reactions perform mildly and cooperatively, the product of the first reaction can be consumed by the second reaction timely, so activating the cascade reaction. The HCM&E is easy to prepare and preserve, and the cost is much less than other

DOI: 10.1021/acsami.5b04398
ACS Appl. Mater. Interfaces 2015, 7, 16694−16705

systems. The high efficiency and good operability of the cascade reaction provides the system great potential applications as a cost-effective biosensors for glucose, and a green catalyst for the oxidation of substrates such as phenols and azo compounds in aqueous media. In addition, HCM&E is an excellent model to construct a multiple-enzyme system tailored to various functions with different types of oxidases. Superoxide dismutase and urate oxidase are also important oxidases that are closely related to physiological activities. They can also be used to construct multiple enzyme systems with new functions when cooperated with hemin-micelles, which may become the focus of our research interests in the future.

■ ASSOCIATED CONTENT

Supporting Information

TEM and SEM images of hydrogels, analysis of solvent effect on gelation, supplementary figures about release kinetics, catalytic analysis, possible mechanism of the inactivation of peroxidases and pictures about cascade reactions. The Supporting Information is available free of charge on the ACS Publications website at DOI: 10.1021/acsami.5b04398.

■ AUTHOR INFORMATION

Corresponding Author

*Tel.: +86 22 23506103. Fax: +86 22 23503510. E-mail: shilinqi@nankai.edu.cn.

Notes

The authors declare no competing financial interest.

■ ACKNOWLEDGMENTS

This work was supported by National Natural Science Foundation of China (No. 91127045), the National Basic Research Program of China (973 Program, No. 2011CB932503), and PCSIRT (No. IRT1257) for the financial support.

■ REFERENCES

(1) Schoffelen, S.; van Hest, J. C. M. Multi-Enzyme Systems: Bringing Enzymes Together *In Vitro*. *Soft Matter* **2012**, *8*, 1736−1746.
(2) Tanner, P.; Balasubramanian, V.; Palivan, C. G. Aiding Nature's Organelles: Artificial Peroxisomes Play Their Role. *Nano Lett.* **2013**, *13*, 2875−2883.
(3) Schrader, M.; Fahimi, H. D. Mammalian Peroxisomes and Reactive Oxygen Species. *Histochem. Cell Biol.* **2004**, *122*, 383−393.
(4) Wanders, R. J. A.; Waterham, H. R. Biochemistry of Mammalian Peroxisomes Revisited. *Annu. Rev. Biochem.* **2006**, *75*, 295−332.
(5) Wilner, O. I.; Weizmann, Y.; Gill, R.; Lioubashevski, O.; Freeman, R.; Willner, I. Enzyme Cascades Activated on Topologically Programmed DNA Scaffolds. *Nat. Nanotechnol.* **2009**, *4*, 249−254.
(6) Rocha-Martin, J.; Velasco-Lozano, S.; Guisan, J. M.; Lopez-Gallego, F. Oxidation of Phenolic Compounds Catalyzed by Immobilized Multi-enzyme Systems with Integrated Hydrogen Peroxide Production. *Green Chem.* **2014**, *16*, 303−311.
(7) Hanefeld, U.; Gardossi, L.; Magner, E. Understanding Enzyme Immobilisation. *Chem. Soc. Rev.* **2009**, *38*, 453−468.
(8) Bäumler, H.; Georgieva, R. Coupled Enzyme Reactions in Multicompartment Microparticles. *Biomacromolecules* **2010**, *11*, 1480−1487.
(9) Logan, T. C.; Clark, D. S.; Stachowiak, T. B.; Svec, F.; Frechet, J. M. J. Photopatterning Enzymes On Polymer Monoliths in Microfluidic Devices for Steady-State Kinetic Analysis and Spatially Separated Multi-enzyme Reactions. *Anal. Chem.* **2007**, *79*, 6592−6598.
(10) Betancor, L.; Berne, C.; Luckarift, H. R.; Spain, J. C. Coimmobilization of a Redox Enzyme and a Cofactor Regeneration System. *Chem. Commun.* **2006**, *42*, 3640−3642.
(11) Kreft, O.; Prevot, M.; Möhwald, H.; Sukhorukov, G. B. Shell-in-Shell Microcapsules: A Novel Tool for Integrated, Spatially Confined Enzymatic Reactions. *Angew. Chem., Int. Ed.* **2007**, *46*, 5605−5608.
(12) Wang, X.; Jiang, Z.; Shi, J.; Liang, Y.; Zhang, C.; Wu, H. Metal-Organic Coordination-Enabled Layer-by-Layer Self-Assembly to Prepare Hybrid Microcapsules for Efficient Enzyme Immobilization. *ACS Appl. Mater. Interfaces* **2012**, *4*, 3476−3483.
(13) Zhang, L.; Shi, J.; Jiang, Z.; Jiang, Y.; Qiao, S.; Li, J.; Wang, R.; Meng, R.; Zhu, Y.; Zheng, Y. Bioinspired Preparation of Polydopamine Microcapsule for Multienzyme System Construction. *Green Chem.* **2011**, *13*, 300−306.
(14) Kuiper, S. M.; Nallani, M.; Vriezema, D. M.; Cornelissen, J. J. L. M.; van Hest, J. C. M.; Nolte, R. J. M.; Rowan, A. E. Enzymes Containing Porous Polymersomes as Nano Reaction Vessels for Cascade Reactions. *Org. Biomol. Chem.* **2008**, *6*, 4315−4318.
(15) Louzao, I.; van Hest, J. C. M. Permeability Effects On the Efficiency of Antioxidant Nanoreactors. *Biomacromolecules* **2013**, *14*, 2364−2372.
(16) Sun, J.; Ge, J.; Liu, W.; Lan, M.; Zhang, H.; Wang, P.; Wang, Y.; Niu, Z. Multi-enzyme Co-embedded Organic−Inorganic Hybrid Nanoflowers: Synthesis and Application as a Colorimetric Sensor. *Nanoscale* **2014**, *6*, 255−262.
(17) Liu, Y.; Du, J.; Yan, M.; Lau, M. Y.; Hu, J.; Han, H.; Yang, O. O.; Liang, S.; Wei, W.; Wang, H.; Li, J.; Zhu, X.; Shi, L.; Chen, W.; Ji, C.; Lu, Y. Biomimetic Enzyme Nanocomplexes and Their Use as Antidotes and Preventive Measures for Alcohol Intoxication. *Nat. Nanotechnol.* **2013**, *8*, 187−192.
(18) Wei, H.; Wang, E. Fe_3O_4 Magnetic Nanoparticles as Peroxidase Mimetics and Their Applications in H_2O_2 and Glucose Detection. *Anal. Chem.* **2008**, *80*, 2250−2254.
(19) Gao, L.; Zhuang, J.; Nie, L.; Zhang, J.; Zhang, Y.; Gu, N.; Wang, T.; Feng, J.; Yang, D.; Perrett, S.; Yan, X. Intrinsic Peroxidase-Like Activity of Ferromagnetic Nanoparticles. *Nat. Nanotechnol.* **2007**, *2*, 577−583.
(20) Gao, Y.; Wei, Z.; Li, F.; Yang, Z. M.; Chen, Y. M.; Zrinyi, M.; Osada, Y. Synthesis of a Morphology Controllable Fe_3O_4 Nanoparticle/Hydrogel Magnetic Nanocomposite Inspired by Magnetotactic Bacteria and its Application in H_2O_2 Detection. *Green Chem.* **2014**, *16*, 1255−1261.
(21) Zhang, Z.; Ma, R.; Shi, L. Cooperative Macromolecular Self-Assembly toward Polymeric Assemblies with Multiple and Bioactive Functions. *Acc. Chem. Res.* **2014**, *47*, 1426−1437.
(22) Shen, L.; Zhao, L.; Qu, R.; Huang, F.; Gao, H.; An, Y.; Shi, L. Complex Micelles with the Bioactive Function of Reversible Oxygen Transfer. *Nano Res.* **2015**, *8*, 491−501.
(23) Qu, R.; Shen, L.; Chai, Z.; Jing, C.; Zhang, Y.; An, Y.; Shi, L. Hemin-Block Copolymer Micelle as an Artificial Peroxidase and Its Applications in Chromogenic Detection and Biocatalysis. *ACS Appl. Mater. Interfaces* **2014**, *6*, 19207−19216.
(24) Hirst, A. R.; Escuder, B.; Miravet, J. F.; Smith, D. K. High-Tech Applications of Self-Assembling Supramolecular Nanostructured Gel-Phase Materials: From Regenerative Medicine to Electronic Devices. *Angew. Chem., Int. Ed.* **2008**, *47*, 8002−8018.
(25) Banwell, E. F.; Abelardo, E. S.; Adams, D. J.; Birchall, M. A.; Corrigan, A.; Donald, A. M.; Kirkland, M.; Serpell, L. C.; Butler, M. F.; Woolfson, D. N. Rational Design and Application of Responsive α-Helical Peptide Hydrogels. *Nat. Mater.* **2009**, *8*, 596−600.
(26) Ikeda, M.; Tanida, T.; Yoshii, T.; Kurotani, K.; Onogi, S.; Urayama, K.; Hamachi, I. Installing Logic-Gate Responses to a Variety of Biological Substances in Supramolecular Hydrogel−Enzyme Hybrids. *Nat. Chem.* **2014**, *6*, 511−518.
(27) Mao, Y.; Su, T.; Wu, Q.; Liao, C.; Wang, Q. Dual Enzymatic Formation of Hybrid Hydrogels with Supramolecular-Polymeric Networks. *Chem. Commun.* **2014**, *50*, 14429−14432.
(28) Sangeetha, N. M.; Maitra, U. Supramolecular Gels: Functions and Uses. *Chem. Soc. Rev.* **2005**, *34*, 821−836.
(29) Ren, C.; Zhang, J.; Chen, M.; Yang, Z. Self-Assembling Small Molecules for the Detection of Important Analytes. *Chem. Soc. Rev.* **2014**, *43*, 7257−7266.

(30) Meazza, L.; Foster, J. A.; Fucke, K.; Metrangolo, P.; Resnati, G.; Steed, J. W. Halogen-Bonding-Triggered Supramolecular Gel Formation. *Nat. Chem.* **2012**, *5*, 42−47.
(31) Gao, W.; Vecchio, D.; Li, J.; Zhu, J.; Zhang, Q.; Fu, V.; Li, J.; Thamphiwatana, S.; Lu, D.; Zhang, L. Hydrogel Containing Nanoparticle-Stabilized Liposomes for Topical Antimicrobial Delivery. *ACS Nano* **2014**, *8*, 2900−2907.
(32) Fan, K.; Niu, L.; Li, J.; Feng, R.; Qu, R.; Liu, T.; Song, J. Application of Solubility Theory in Bi-component Hydrogels of Melamine with Di(2-Ethylhexyl) Phosphoric Acid. *Soft Matter* **2013**, *9*, 3057−3062.
(33) Manna, S.; Saha, A.; Nandi, A. K. A Two Component Thermoreversible Hydrogel of Riboflavin and Melamine: Enhancement of Photoluminescence in the Gel Form. *Chem. Commun.* **2006**, *42*, 4285−4287.
(34) Saha, A.; Manna, S.; Nandi, A. K. Hierarchical Tuning of 1-D Macro Morphology by Changing the Composition of a Binary Hydrogel and its Influence On the Photoluminescence Property. *Chem. Commun.* **2008**, *44*, 3732−3734.
(35) Zhang, J.; Ou, C.; Shi, Y.; Wang, L.; Chen, M.; Yang, Z. Visualized Detection of Melamine in Milk by Supramolecular Hydrogelations. *Chem. Commun.* **2014**, *50*, 12873−12876.
(36) Paquet, C.; de Haan, H. W.; Leek, D. M.; Lin, H.; Xiang, B.; Tian, G.; Kell, A.; Simard, B. Clusters of Superparamagnetic Iron Oxide Nanoparticles Encapsulated in a Hydrogel: A Particle Architecture Generating a Synergistic Enhancement of the T-2 Relaxation. *ACS Nano* **2011**, *5*, 3104−3112.
(37) Xu, Y.; Wu, Q.; Sun, Y.; Bai, H.; Shi, G. Three-Dimensional Self-Assembly of Graphene Oxide and DNA into Multifunctional Hydrogels. *ACS Nano* **2010**, *4*, 7358−7362.
(38) Chen, Y.; Pang, X.; Dong, C. Dual Stimuli-Responsive Supramolecular Polypeptide-Based Hydrogel and Reverse Micellar Hydrogel Mediated by Host−Guest Chemistry. *Adv. Funct. Mater.* **2010**, *20*, 579−586.
(39) Larsen, R. W.; Wojtas, L.; Perman, J.; Musselman, R. L.; Zaworotko, M. J.; Vetromile, C. M. Mimicking Heme Enzymes in the Solid State: Metal-Organic Materials with Selectively Encapsulated Heme. *J. Am. Chem. Soc.* **2011**, *133*, 10356−10359.
(40) Lee, C.; Lin, T.; Mou, C. Mesoporous Materials for Encapsulating Enzymes. *Nano Today* **2009**, *4*, 165−179.
(41) Xiao, L.; Zhu, J.; Londono, J. D.; Pochan, D. J.; Jia, X. Mechano-Responsive Hydrogels Crosslinked by Block Copolymer Micelles. *Soft Matter* **2012**, *8*, 10233−10237.
(42) Sun, Y.; Gao, G.; Du, G.; Cheng, Y.; Fu, J. Super Tough, Ultrastretchable, and Thermoresponsive Hydrogels with Functionalized Triblock Copolymer Micelles as Macro-cross-linkers. *ACS Macro Lett.* **2014**, *3*, 496−500.
(43) Chung, J. W.; An, B.; Park, S. Y. A Thermoreversible and Proton-Induced Gel-Sol Phase Transition with Remarkable Fluorescence Variation. *Chem. Mater.* **2008**, *20*, 6750−6755.
(44) Roy, B.; Bairi, P.; Saha, A.; Nandi, A. K. Variation of Physical and Mechanical Properties in the Bicomponent Hydrogels of Melamine with Positional Isomers of Hydroxybenzoic Acid. *Soft Matter* **2011**, *7*, 8067−8076.
(45) Bairi, P.; Roy, B.; Chakraborty, P.; Nandi, A. K. Co-assembled White-Light-Emitting Hydrogel of Melamine. *ACS Appl. Mater. Interfaces* **2013**, *5*, 5478−5485.
(46) Hoare, T. R.; Kohane, D. S. Hydrogels in Drug Delivery: Progress and Challenges. *Polymer* **2008**, *49*, 1993−2007.
(47) Lin, C.; Anseth, K. S. PEG Hydrogels for the Controlled Release of Biomolecules in Regenerative Medicine. *Pharm. Res.* **2009**, *26*, 631−643.
(48) Tessmar, J. K.; Göpferich, A. M. Matrices and Scaffolds for Protein Delivery in Tissue Engineering. *Adv. Drug Delivery Rev.* **2007**, *59*, 274−291.
(49) Lin, C.; Metters, A. T. Hydrogels in Controlled Release Formulations: Network Design and Mathematical Modeling. *Adv. Drug Delivery Rev.* **2006**, *58*, 1379−1408.
(50) Gupta, P.; Vermani, K.; Garg, S. Hydrogels: From Controlled Release to pH-responsive Drug Delivery. *Drug Discovery Today* **2002**, *7*, 569−579.
(51) Ritger, P. L.; Peppas, N. A. A Simple Equation for Description of Solute Release I. Fickian and Non-Fickian Release from Non-Swellable Devices in the Form of Slabs, Spheres, Cylinders or Discs. *J. Controlled Release* **1987**, *5*, 23−36.
(52) Ashley, G. W.; Henise, J.; Reid, R.; Santi, D. V. Hydrogel Drug Delivery System with Predictable and Tunable Drug Release and Degradation Rates. *Proc. Natl. Acad. Sci. U. S. A.* **2013**, *110*, 2318−2323.
(53) Siepmann, J.; Peppas, N. A. Higuchi Equation: Derivation, Applications, Use and Misuse. *Int. J. Pharm.* **2011**, *418*, 6−12.
(54) Ritger, P. L.; Peppas, N. A. A Simple Equation for Description of Solute Release II. Fickian and Anomalous Release From Swellable Devices. *J. Controlled Release* **1987**, *5*, 37−42.
(55) Adediran, S. A.; Lambeir, A. M. Kinetics of the Reaction of Compound II of Horseradish Peroxidase with Hydrogen Peroxide To Form Compound III. *Eur. J. Biochem.* **1989**, *186*, 571−576.
(56) Wariishi, H.; Gold, M. H. Lignin Peroxidase Compound III. Mechanism of Formation and Decomposition. *J. Biol. Chem.* **1990**, *265*, 2070−2077.
(57) Valderrama, B.; Ayala, M.; Vazquez-Duhalt, R. Suicide Inactivation of Peroxidases and the Challenge of Engineering More Robust Enzymes. *Chem. Biol.* **2002**, *9*, 555−565.
(58) Winkel, B. S. J. Metabolic Channeling in Plants. *Annu. Rev. Plant Biol.* **2004**, *55*, 85−107.
(59) Sherman, M. R.; Saifer, M. G. P.; Perez-Ruiz, F. PEG-uricase in the Management of Treatment-Resistant Gout and Hyperuricemia. *Adv. Drug Delivery Rev.* **2008**, *60*, 59−68.
(60) Kehrer, J. P. Free Radicals as Mediators of Tissue Injury and Disease. *Crit. Rev. Toxicol.* **1993**, *23*, 21−48.
(61) Xue, T.; Peng, B.; Xue, M.; Zhong, X.; Chiu, C.; Yang, S.; Qu, Y.; Ruan, L.; Jiang, S.; Dubin, S.; Kaner, R. B.; Zink, J. I.; Meyerhoff, M. E.; Duan, X.; Huang, Y. Integration of Molecular and Enzymatic Catalysts On Graphene for Biomimetic Generation of Antithrombotic Species. *Nat. Commun.* **2014**, *5*, 3200.
(62) Wang, Q.; Yang, Z.; Zhang, X.; Xiao, X.; Chang, C. K.; Xu, B. A Supramolecular-Hydrogel-Encapsulated Hemin as an Artificial Enzyme to Mimic Peroxidase. *Angew. Chem., Int. Ed.* **2007**, *46*, 4285−4289.
(63) Sang, S.; Yang, C. S.; Ho, C. Peroxidase-Mediated Oxidation of Catechins. *Phytochem. Rev.* **2004**, *3*, 229−241.
(64) Richard-Forget, F. C.; Gauillard, F. A. Oxidation of Chlorogenic Acid, Catechins, and 4-Methylcatechol in Model Solutions by Combinations of Pear (*Pyrus Communis* Cv. Williams) Polyphenol Oxidase and Peroxidase: A Possible Involvement of Peroxidase in Enzymatic Browning. *J. Agric. Food Chem.* **1997**, *45*, 2472−2476.
(65) Hosny, M.; Rosazza, J. Novel Oxidations of (+)-Catechin by Horseradish Peroxidase and Laccase. *J. Agric. Food Chem.* **2002**, *50*, 5539−5545.
(66) Campos-Martin, J. M.; Blanco-Brieva, G.; Fierro, J. L. G. Hydrogen Peroxide Synthesis: An Outlook Beyond the Anthraquinone Process. *Angew. Chem., Int. Ed.* **2006**, *45*, 6962−6984.

DOI: 10.1021/acsami.5b04398
ACS Appl. Mater. Interfaces 2015, 7, 16694−16705